Journal of Controlled Release 327 (2020) 88–99

Contents lists available at ScienceDirect

Journal of Controlled Release

journal homepage: www.elsevier.com/locate/jconrel

Galactosylated chitosan-modified ethosomes combined with silk fibroin nanofibers is useful in transcutaneous immunization

Xingxing Yang[a,1], Xiaoyun Wang[c,1], Huoyan Hong[a,1], Gomaa Elfawal[a,e], Si Lin[a], Jinglei Wu[a], Yuxin Jiang[b,*], Chuanglong He[a], Xiumei Mo[a], Guoyin Kai[d,*], Hongsheng Wang[a,*]

[a] Key Laboratory of Science & Technology of Eco-Textile, Ministry of Education, College of Chemistry, Chemical Engineering and Biotechnology, Donghua University, Shanghai 201620, PR China
[b] Department of Pathogenic Biology and Immunology, School of Medicine, Jiaxing University, Jiaxing 314001, PR China
[c] Department of Obstetrics & Gynecology, Shanghai First People's Hospital Affiliated to Shanghai Jiaotong University, Shanghai 201620, PR China
[d] Laboratory of Medicinal Plant Biotechnology, College of Pharmaceutical Sciences, Zhejiang Chinese Medical University, Hangzhou 311402, PR China.
[e] Polymer Materials Research Department, Advanced Technology and New Materials Research Institute (ATNMRI), City of Scientific Research and Technological Applications (SRTA-City), Alexandria, Egypt

ARTICLE INFO

Keywords:
Transcutaneous immunization
Dendritic cells
Ethosome
Galactosylated chitosan
Hyaluronic acid
Silk fibroin
Electrospinning

ABSTRACT

Transcutaneous immunization (TCI) has the advantages of avoiding the liver first-pass effect, good compliance and convenient use compared with the traditional oral or injection vaccination. However, the stratum corneum (SC) of the skin is the main obstacle that limits the entry of antigen molecules into the epidermis for activating dendritic cells (DCs). In the present study, the hyaluronic acid (HA) and galactosylated chitosan (GC) modified ethosome (Eth-HA-GC) was prepared through layer-by-layer self-assembly method. Eth-HA-GC has good stability and can be effectively phagocytosed by the bone-marrow-derived DCs (BMDCs) in vitro. The ovalbumin (OVA) loaded Eth-HA-GC (OVA@Eth-HA-GC) can promote BMDCs' expression of CD80, CD86 (DCs maturation-associated marker molecules), TNF-α, IL-2 and IL-6. Subsequently, a novel OVA@Eth-HA-GC-loaded silk fibroin (OVA@Eth-HA-GC/SF) nanofibrous mats were fabricated through green electrospinning. The OVA@Eth-HA-GC/SF mats exhibit good transdermal performance in vitro. Transdermal administration with OVA@Eth-HA-GC/SF mats induced the serum anti-OVA-specific IgG and increased the expression of IFN-γ, IL-2 and IL-6 by spleen cells in vivo. Furthermore, the use of OVA@Eth-HA-GC/SF mats evidently inhibited the growth of EG7 tumor in the murine model. These results demonstrate the OVA@Eth-HA-GC/SF mats can effectively stimulate the immune response to OVA through transdermal administration. In conclusion, the antigens@Eth-HA-GC/SF mats is a promising TCI system.

1. Introduction

Transcutaneous immunization (TCI) provides an alternative method to safe and effective vaccination through intact or pretreated skin instead of normal methods such as subcutaneous injection (s.c.), intramuscular injection (i.m.), or oral administration methods [1,2]. TCI avoid drug degradation in liver and/or gastrointestinal route and it is painless [1,2]. TCI can achieve similar effects at lower doses compared with s.c. or i.m. injections, because the skin has plentiful antigen-presenting cells (APCs) - mainly dendritic cells (DCs) that priming naive T cells and elicit an efficient adaptive immune response via capturing and presenting antigens [1–3]. However, the stratum corneum (SC), in the outermost of the epidermis, forms an almost fully impermeable barrier that prevents the pathogen invasion and antigen with a molecular weight larger than 500 Da to pass [4,5]. Thus, increasing the efficiency of transdermal administration is an urgent issue.

Ethosomes (Eths) have been used as a transdermal carrier to increase the drug delivery efficiency due to its excellent capacity of liquidity, deformability and the high encapsulation ability [5–8]. Eth is a special liposome, named after the introduction of alcohol [8]. The presence of alcohol imparts higher fluidity and deformability to Eth, thereby significantly improving its transdermal ability [9–12]. For transdermal drug delivery products, the patch has advantages of easy to use and store compared with the liquid formulation. The nanofibrous mats are a good substrate for drug delivery – it has large specific surface area that provides more contact sites for cells – as the loaded drugs are

* Corresponding authors.
E-mail addresses: jiangyx@zjxu.edu.cn (Y. Jiang), kaiguoyin@zcmu.edu.cn (G. Kai), whs@dhu.edu.cn (H. Wang).
[1] Authors contributed equally

https://doi.org/10.1016/j.jconrel.2020.07.047
Received 19 November 2019; Received in revised form 28 July 2020; Accepted 30 July 2020
Available online 05 August 2020
0168-3659/

easily taken up by cells [13,14]. Studies have also shown that nanocarriers attached to the nanofibers not only have a significantly improved stability but also a smoother release of the drug contained therein [15]. Silk fibroin (SF) is a natural biomacromolecules with excellent biocompatibility, good water retention, gas permeability and skin affinity [16,17]. Also, SF nanofibers can well mimic the extracellular matrix [16,17]. Thus, the Eths-loaded SF nanofibrous mats can be a useful system for transdermal drug delivery.

Modification of the antigen-carriers to target DCs is helpful to improve the immune efficiency of the vaccination system [18–20]. The galactose-type C-type lectin (GCL) on the surface of DCs in humans and mice is a type II transmembrane glycoprotein that can bind galactose, *N*-acetyl galactosamine, Lewis X (such as monosaccharides), and oligosaccharides [21,22]. The galactosyl groups have a high affinity for mouse GCLs receptors and therefore it is considered as an effective ligand that can target DCs [19,20]. The Galactosylated chitosan (GC) contained scaffolds has been proved beneficial to the attachment and proliferation of liver cells for their specific recognition and interaction [23–25]. GC can be used for targeting DCs as it contains galactosyl and has the advantages of biodegradability and biocompatibility [23–25]. Hyaluronic acid (HA) is an important constituent of the extracellular matrix with high concentrations in the skin and has been proved to be a useful carrier material for transdermal delivery [26–28]. HA-modified Eths showed an improved performance on both stability and skin permeation compared with the bare Eths [26]. Therefore, we hypothesize that the SF nanofibrous mats loaded with HA and GC modified Eths could be an ideal solution for TCI.

In this study, we prepared HA & GC-modified Eths (Eth-HA-GC) through layer-by-layer self-assembly to form an antigens delivery system which can effectively deliver antigens to the DCs. The ovalbumin (OVA) was used as model drug to observe the performance of Eth-HA-GC on targeting and activating DCs. Subsequently, a novel TCI system based on the Eth-HA-GC-loaded SF (Eth-HA-GC/SF) nanofibrous patch was developed to facilitate the use of Eth-HA-GC. Morphology of Eth-HA-GC/SF was characterized with both scanning electron microscope (SEM) and confocal laser scanning microscopy (CLSM). The transcutaneous performance of the OVA-loaded Eth-HA-GC/SF (OVA@Eth-HA-GC/SF) was determined by in vitro test with mouse isolated skin. The transdermal immunological efficiency of OVA@Eth-HA-GC/SF was evaluated with mice models by detecting the levels of IGG, IFN-γ, IL-2 and IL-6. Furthermore, the OVA@Eth-HA-GC/SF was used to treat the tumor-bearing mice models which were in advance subcutaneously inoculated with E.G7-OVA cells to directly observe its immune effect.

2. Experimental section

2.1. Materials

Fluorescein isothiocyanate (FITC), 3-(4,5-dimethyl-2-thiazolyl)-2,5-diphenyl-2-H-tetrazolium bromidecholesterol (MTT), 1,10-dioctadecyl-3,3,30,30-tetramethylindocarbocyanine perchlorate (DiI), 4,6-diamino-2-phenylindole dihydrochloride (DAPI), lithium bromide (LiBr), lecithin, cholesterol, octadecylamine, sodium forms of HA (Mw = 30–50 kDa), chitosan (Mw = 50–190 kDa), poly(ethylene oxide) (PEO, Mw = 900 kDa), Dimethyl Sulfoxide (DMSO), lipopolysaccharide (LPS), Rhodamine-labeled phalloidin, and OVA were purchased from Sigma-Aldrich (Shanghai) Trading Co., Ltd. (China). Cocoons of *B. mori* silkworm were from Huzhou Silk Co., Ltd. (China). Lactose acid (LA) and *N*,*N*,*N*′,*N*′-Tetramethylethylenediamine (TEMED) were from Sangon Biotechnology (Shanghai) Co., Ltd. (Shanghai, China). N-(3-(dimethylamino)-propyl)-3-ethylcarbodiimide hydrochloride (EDC) and N-Hydroxysuccinimide (NHS) were from Sinopharm Chemical Reagent Co. Ltd. (Shanghai, China). RPMI 1640 medium, high-sugar DMEM medium and fetal bovine serum (FBS) were from Gibco (USA). Granulocyte macrophage colony-stimulating factor (GM-CSF), IL-4, PE-labeled goat anti-mouse (CD11c, CD80, CD86) monoclonal antibodies and TMB ELISA kits (for detection of IgG, IL-2, IL-6, TNF-α and IFN-γ) were from PeproTech (USA). L929 cell line was provided by the Institute of Biochemistry and Cell Biology Sciences, Chinese Academy of Sciences (Shanghai, China). E.G7-OVA cells were from Shanghai jiwei Biological technology co., Ltd. (China). C57BL/6 mice were purchased from Shanghai SLAC Laboratory Animal Co. Ltd. (Shanghai, China). Ultrapure water was used throughout this study.

2.2. Synthesis of Galactosylated chitosan

GC was prepared as previously described [25]. Briefly, 2.3 g of LA dissolved in 50 mL of TEMED/HCl buffer solution (pH = 4.7) was successively activated by mixture of 0.14 g EDC and 0.6 g of NHS. Then, 2.2 g of chitosan (2-fold molar over LA) was added and reacted for 72 h at room temperature (RT). The product was purified by dialysis in water for 3 days at RT. Finally, lyophilized GC was identified through attenuated total reflection-fourier transform infrared spectroscopy (ATR-FTIR) (Nexus-670, Hitachi, Japan).

2.3. Preparation and characterization of the galactosylated eths

The Eths were prepared as reported earlier [29]. Briefly, 100 mg egg yolk lecithin, 10 mg cholesterol, and 4 mg octadecylamine were dissolved in 5 mL of absolute ethanol at room temperature, and remove the ethanol by rotary evaporation at 40 °C to obtain a lipid film. The films were then rehydrated with 10 mL 20% ethanol containing 0 or 0.1 mg/mL drugs (OVA or FITC-labeled OVA (FITC-OVA)) through agitating for 30 min at RT. Homogeneous OVA-loaded cationic Eths were obtained using a probe sonicator (JY92-II, NingBo Scientz Biotechnology Co., Ltd., Ningbo, China), and non-encapsulated free drugs were removed by centrifugation. Then, the solution was filtered with a 220 nm microporous filter membrane for several times to obtain Eths with a uniform particle size. The Eths were then coated with equal volume of 1 mg/mL HA aqua solution at RT for 2 h to obtain HA-coated Eths (Eths-HA), centrifugated to remove the free HA. Subsequently, an equal volume of Eth-HA and 1% (*w/v*) GC acetic acid solution (pH = 4.0) were mixed and stirred at RT for 2 h. After removing the free GC by centrifugation, the Eth-HA-GC was obtained. DiI-labeled Eths were prepared by adding 0.2 mL DiI (10 Mm ethanol solution) to 10 mL Eths solution. Stirring the mix solution for half an hour and the DiI-labeled Eth was obtained after dialysis for three days (changing water 3 times a day) against deionized water. Free DiI and DiI aggregates were removed by centrifugation. Eth, Eth-HA and Eth-HA-GC were characterized by Zeta potentials (Malvern Instruments, UK), laser particle analyzer (BI-200SM, Brookhaven, USA), and transmission electron microscopy (TEM) (JEM-2100, JEOL Ltd., Japan) - at an acceleration voltage of 200 kV with a LaB_6 electron gun.

2.4. Assays of cellular uptake of the eths and the induction of DCs in vitro

Mouse bone-marrow-derived dendritic cells (BMDCs) were isolated according to a reported protocol [30]. Briefly, the bone marrow cells were isolated from both shinbones and thighbones of female C57BL/6 mice (6–8 weeks old). The marrow cells were cultured in RPMI 1640 complete medium supplemented with 10% FBS, 100 U/mL penicillin and 100 μg/mL streptomycin, 1000 U/mL GM-CSF and 500 U/mL IL-4 in a 5% CO_2 incubator at 37 °C under a humid atmosphere. Suspended BMDCs were harvested after 6 or 7 days of culture.

To investigate the ability of the modified Eths to target DCs, the BMDCs were seeded in 35 mm glass bottom dishes (5×10^4 per dish) and co-cultured with 40 μL DiI-labeled Eths (30 μg/mL) in the dark for 2 h, the untreated cells were used as control. Then, cells were washed with PBS for 3 times and fixed with 4% paraformaldehyde for 30 min. Subsequently, cells were stained with DAPI for 10 min, washed with PBS 3 times, observed under a confocal laser scanning microscope

(ZEISS LSM 700, Jena, Germany).

To further quantitatively analyze the phagocytosis of Eths by DCs, BMDCs were seeded in a 24-well plate (1×10^5 per well) and further co-cultured with free FITC-OVA, FITC-OVA loaded ethosomes (FITC-OVA@Eth), FITC-OVA loaded Eth-HA (FITC-OVA@Eth-HA), or FITC-OVA loaded Eth-HA-GC (FITC-OVA@Eth-HA-GC) for 12 h. Subsequently, the cells were slightly washed with sterile PBS three times to discard redundant free FITC-OVA or various Eths. The uptake efficiency of BMDCs was measured immediately by flow cytometry under a FACSCalibur (Becton Dickinson, USA).

To evaluate the changed ability of BMDCs induced by the OVA-loaded Eths, the suspended BMDCs (1×10^5 per well) were incubated in 24-well plate with OVA@Eth, OVA@Eth-HA, or OVA@Eth-HA-GC respectively for 24 h, LPS treated cells were used as control. Cells were then harvested and incubated with PE-goat anti-mouse CD11c, CD80 or CD86 monoclonal antibodies for 30 min. The expression of CD11c, CD80 and CD86 by BMDCs were detected with flow cytometry under a FACSCalibur (Becton Dickinson, USA). The concentrations of TNF-α, IL-2 and IL-6 in the supernatant of each sample were also determined with TMB ELISA kits.

2.5. Preparation and characterization of the eths-loaded SF nanofibrous mats (ESNFM)

SF was prepared using the method described in our previous study [17,31]. Briefly, cocoons were boiled three times (30 min/time) in a 0.5% (wt/v) Na_2CO_3 aqueous solution, and then sericin was removed by rinsing with ultrapure water. The degummed and dried silk was dissolved in 9.3 M LiBr solution in a water bath at 45 °C for 30 min. Then, the homogeneous solution was dialyzed (molecular weight cutoff = 14.000 Da) against deionized water for 3 days. Finally, the regenerated SF sponges was gained by filtering and lyophilizing the SF solution.

The nanofibers were prepared via the similar eco-friendly process as described in our previous studies [17,31]. Briefly, 1.0 g SF, 0.1 g PEO and 0.25 g OVA (free or loaded in ethosomes) dissolved together in 5 mL ultrapure water and the mixture was stirred over 12 h to obtain stable spinning solutions. The solutions were then electrospun at a stable extruding rate of 1.0 mL/h under a voltage of +12 kV and the collect distance was 15 cm. The resulting products were dried and stored under vacuum at room temperature before use. The surface morphology of the nanofibrous mats was observed using scanning electron microscope (SEM) and the distribution of the FITC-OVA-loaded Eths on the SF nanofibers was observed by fluorescence microscopy.

2.6. Cytocompatibility assays

The nanofibrous patches were collected on circle glasses (14 mm in diameter) for cellular study. After treated with 75% (v/v) ethanol vapor for 24 h, the fiber-deposited glasses were placed into a 24-well culture plate without further sterilizing, and fixed with autoclaved stainless steel rings, with fiber-free glasses as controls. Mouse fibroblast L929 cells were seeded on the nanofibrous matrices at a density of 2×10^4 cells/well and cultured with high-sugar DMEM medium supplemented with 10% (v/v) FBS and 1% (v/v) penicillin/streptomycin and incubated in a humidified incubator at 37 °C with 5% CO_2.

For cell viability assay, cells were washed once with PBS buffer after culturing for 1, 3, or 5 days. Then, 360 μL of the culture medium containing no serum and 40 μL of MTT solution (5 mg/mL) were added to each well and incubated for another 4 h at 37 °C in the 5% CO_2 incubator. The medium was discarded, and 400 μL of DMSO was added to each well, shaking for 30 min. at room temperature in the dark. The absorbance at the 492 nm was measured using a microplate reader (Multiskan MK3, Thermo). Each group was repeated 3 times with a slide as a blank control.

For cell morphology, after 3 days of culture, cells were washed 3 times with PBS, and then fixed with 4% paraformaldehyde at 4 °C for 2 h. The supernatant was discarded and the cells were washed 3 times with PBS. Cells were subjected to gradient dehydration with ethanol and then treated under vacuum spray, the morphology of the cells was observed by SEM. Moreover, the paraformaldehyde-fixed cells were treated with 0.1% Triton solution for 3–5 min. and washed 3 times with PBS. Then, the samples were treated with 2% (wt/v) bovine serum albumin (BSA) solution for 20–30 min. and washed with PBS 3 times. Rhodamine-labeled phalloidin (5μg/mL) was added onto the slides for 30 mins' staining in the dark and wash with PBS for 3 times. Finally, DAPI was added to stain for 5 min. in the dark and wash with PBS for 3 times. The morphology of cells was observed under fluorescence microscope.

2.7. Assays to assess the transdermal performance of the ESNFM in vitro

The hairs on the abdomen were removed from dead mice by a razor and the full thickness of abdominal skin was surgically peeled off. The subcutaneous fat was removed from the dermis side with surgical scissors. The obtained skin was then repeatedly washed with sterile PBS (pH = 7.4) until no turbidity and stored at −20 °C for further use.

The Franz diffusion cells were used to investigate the transdermal performance of the ESNFM in vitro (Fig. 1). The above prepared skin

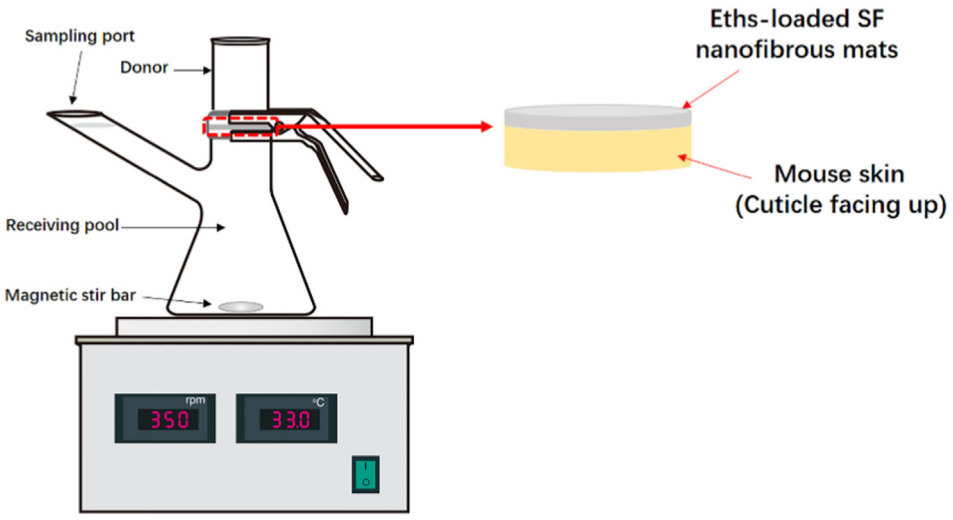

Fig. 1. Scheme of in vitro skin permeation assay using the Franz diffusion cell.

(the surface of stratum corneum facing up) was sandwiched between the donor and receiving pool of the diffusion cell system, and the ESNFMs loaded with FITC-OVA were tightly attached to the surface of the skin. The receiving pool was filled with PBS (pH = 7.4), which was stirred continuously at 350 rpm and maintained at the temperature of 33 °C by water bath. At appropriate interval (0.5, 1, 2, 4, 6, 8, 10, 12, 24, 36, 48 h respectively), 2 mL of the receiving solution was withdrawn via the sampling port and then replaced by equal volume of fresh buffer. The absorbance value of the receiving solution at 488 nm was detected with a UV–vis spectrophotometer (UV1100, TECHCOMP, China), and the cumulative drug permeation (Q) through the skin was calculated according to the FITC standard curve and the following formula:

$$Q = \frac{VC_n + \Sigma_{i=1}^{n-1} C_i V_i}{Q'} \times 100\%$$

Where V is the volume of the transdermal cup, C_n is the drug concentration of the receiver solution at each test time, C_i is the drug concentration of the i-th sample, Vs is the sample volume and Q' is the total amount of drug in the ESNFM.

The skin was removed from the Franz diffusion cell after the above transdermal experiment and made into paraffin sections with a thickness of approximately 10 μm. FITC-OVA distribution in paraffin section was observed by a fluorescent microscope (TS10, Nikon, Japan).

2.8. Animal experiments

Six-week-old C57BL/6 female mice were maintained in a 12 h light/dark cycle with free access to food and water (SPF environment). All animal experiments were performed according to the guidelines approved by the Institutional Animal Care and Use Committee at Donghua University.

2.9. Transcutaneous immunization of mice with ESNFM

Mice were randomly divided into five groups of 10 mice in each group. Before immunization, the abdomen fur of each mouse was shaved with an area of about 2 cm × 2 cm. Then the mice were anesthetized by intraperitoneal injection of 0.2 mL pentobarbital solution. After moistened with a little PBS, the nanofibrous mats containing 10 μg of OVA were attached to the abdomen shaving area and fixed with medical tape to make the mats in close contact with the skin for 48 hs. The same operation was repeated to boost the immunization on the 14th day.

Blood samples were collected from eye venous plexus (0.5 mL for each mouse) on days 14 and 28 after the first immunization, respectively. Serum were isolated from the blood samples by further standing for 30 min at RT and then centrifugation for 5 min at 3000 rpm. Firstly, the ELISA plates were coated with 100 μL OVA solution (10 μg/mL) overnight at 4 °C, and unbound OVA was removed by washing 3 times using 300 μL TPBS. Subsequently, the plates were blocked with 100 μL TPBS solution containing 1% BSA in a 37 °C incubator for 1 h. Each well was added 100 μL of 2-fold serially diluted samples. To detect the IgG, 100 μL of 1: 5000 diluted goat anti-mouse IgG-HRP monoclonal antibody was added and TME color developing solution was used to color development. Finally, 100 μL 2 M H_2SO_4 solution was added to each well to terminate color development. A microplate reader (Multiskan MK3, Thermo) was used to detect absorption value at 450 nm.

Mice immunized for 28 days as described above were killed by cervical dislocation. Their spleens were taken out and cut into pieces and digested with collagenase until the cells were dispersed. Cell suspension was then collected and centrifuged at 1200 rpm for 5 min, discarding the supernatant and the red blood cell lysate was added for resuspension. After standing for 2 min, the fragments of red blood cells were removed by centrifugation at 1500 rpm for 5 min. Cells were washed with PBS for 3 times, and suspended with RPMI 1640 medium containing 10% FBS and 1% penicillin-streptomycin, transferred to the 6-well plate and cultured in the incubator for 48 h. Then the culture medium was completely discarded and the cells were resuspended with RPMI 1640 medium and adjusted to 1 × 10^5/mL. Cells were treated with OVA (10 μ g/mL) and continue to culture for 24 h. The supernatant was extracted to detect levels of IFN - γ, IL-2 and IL-6 with the TMB ELISA kits.

2.10. Tumor-bearing experiment in mice after transcutaneous immunization

Mice were randomly divided into five groups of 5 mice in each group and transdermal immunized as described in the previous method. On days 14 after the second immunization, each mouse were subcutaneously inoculated with 5 × 10^5 E.G7-OVA cells (mouse T lymphocytes). Tumor growth was observed every day after inoculation, and the length (L) and width (W) of the tumor were measured with a vernier caliper every 4 days and recorded. Tumor volume (V) was calculated using the following equation: V = 0.5 × L × W^2.

2.11. Statistical analysis

All data were reported as mean ± standard deviation. Statistical analysis was conducted using the one-way analysis of variance (ANOVA). a p-value < 0.05 was considered significant, and the data were indicated with * (or #) for $p < 0.05$, ** (or ##) for $p < 0.01$ and *** (or ###) for $p < 0.001$.

3. Results

3.1. Characterization of Galactosylated ethosomes

FTIR spectroscopy was used to investigate the structural variation during the preparation of the Eth-HA-GC (Fig. 2). The cationic Eths with positive charged surface were firstly prepared using octadecylamine by film dispersion method [29]. Subsequently, HA was conjugated onto the surface of the cationic Eths through electrostatic adsorption and change the surface into negative charged one. Finally, the GC was coated onto the negative charged Eth-HA to obtain the Eth-HA-GC. As shown in Fig. 2, HA showed peaks at 3409.9 cm^{-1} that confirms the presence of OH and at 2897.7 cm^{-1} due to the C—H stretching, 1618.5 cm^{-1} that indicates the presence of amid II group, at 1417.73 cm^{-1} that refer to C—O group with C═O combination, and 1049.5 cm^{-1} refer to the C-O-C stretching. Those results agree with earlier FTIR for HA [32]. FTIR for Eth shows peaks at 2880.6 cm^{-1}

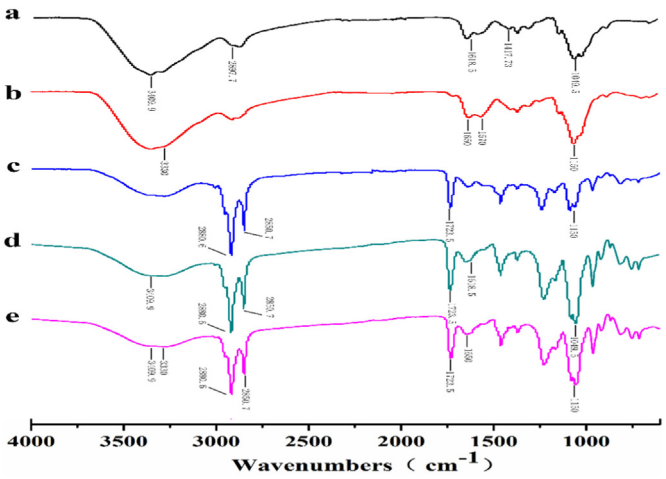

Fig. 2. Infrared spectrum of the Eths (a: HA; b: GC; c: Eth; d: Eth-HA; e: Eth-HA-GC).

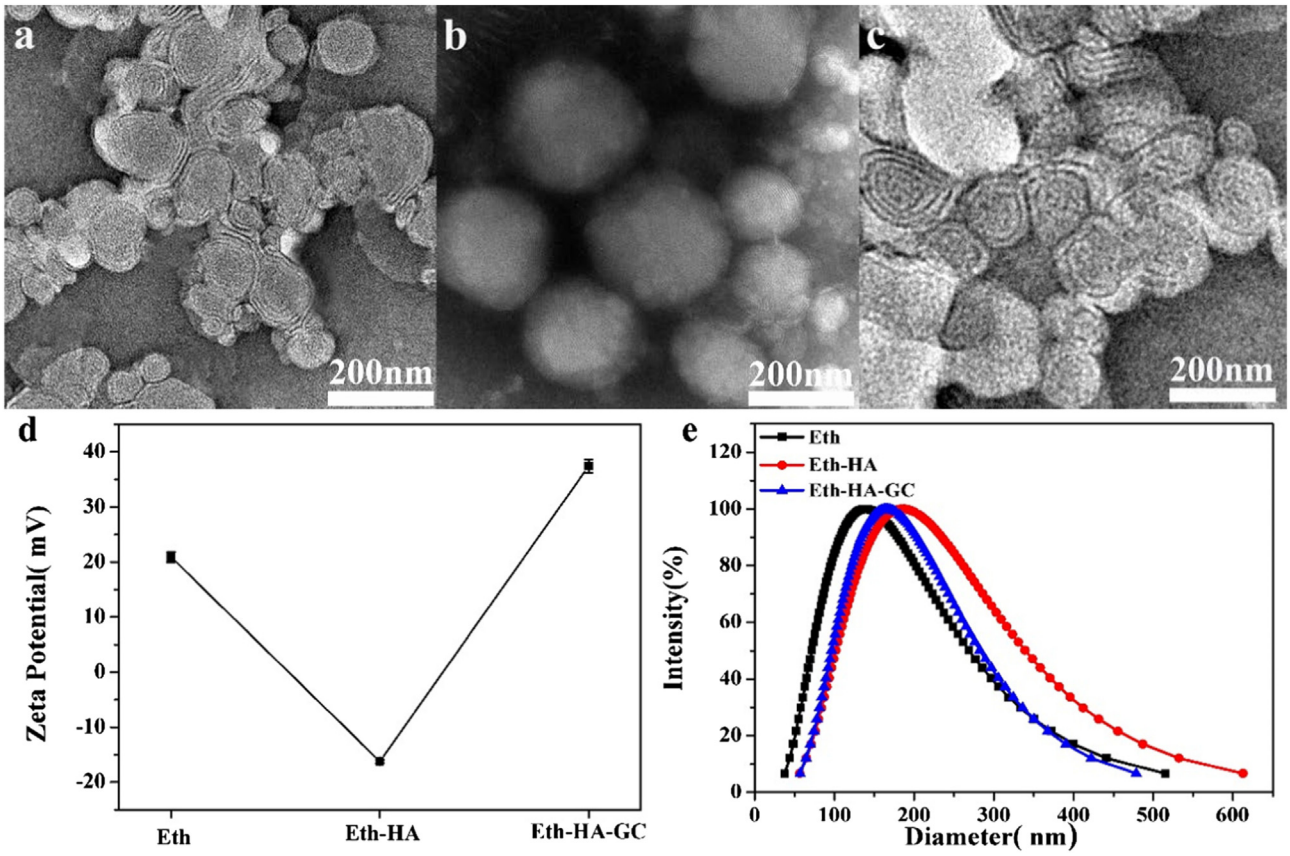

Fig. 3. TEM images (a, b, c), zeta potentials (d) and diameters (e) of the Eth, Eth-HA and Eth-HA-GC (a: Eth; b: Eth-HA; c: Eth-HA-GC).

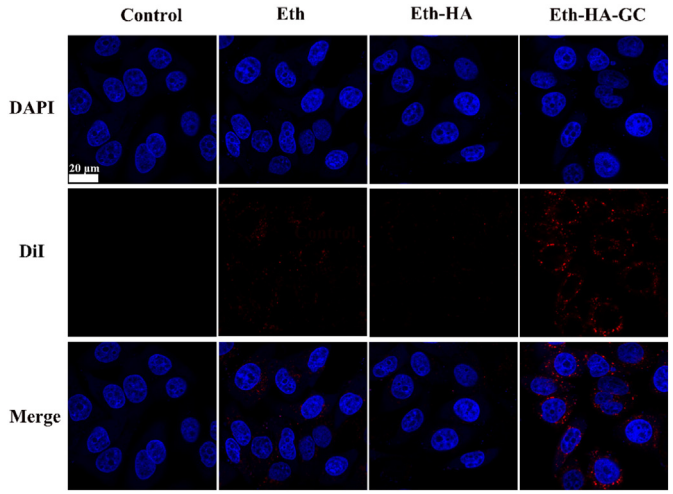

Fig. 4. Confocal laser scanning microscopy images of DCs phagocytosing DiI-labeled Eths.

refer to CH_2 stretch, at 2850.7 cm^{-1} refer to C—H and peak at 1723.5 cm^{-1} refer to C═O. Those results agree with earlier FTIR for Eth [33]. GC spectrum show peaks at 1650 cm^{-1} refer to the acylamino group, at 1570 cm^{-1} refer to the unreacted amino groups, at 1150 cm^{-1} refer to C-O-C bridge, and at 3330 cm^{-1} refer to hydroxyl groups [34]. The Eth-HA show the peaks of HA and Eth with small intensity changes, suggesting that HA is successfully adsorbed on the ethosomes. Similarly, the spectrum of the Eth-HA-GC has the characteristic peaks of HA, GC and Eth, implying that GC is successfully adsorbed on the surface of the Eths.

The TEM image shows a spherical morphology with a multi-layer cystic structure for the bare Eth with a diameter around 120 nm (Fig. 3a). After modification by HA, the diameter was increased to about 200 nm and the inner cystic structure became fuzzy (Fig. 3b**&e**). The surface change of the Eth-HA was presumably due to the coating of hydrophilic HA [35]. In contrast, the Eth-HA-GC shows a decreased diameter compared to the Eth-HA, which might be due to the highly dense form between HA and GC (Fig. 3c&e) [36]. In addition, the poly dispersity index (PDI) values of the particles were 0.364, 0.325 and 0.25 for Eth, Eth-HA and Eth-HA-GC, respectively. The entrapment efficiency of the prepared Eths to OVA was 63.58% ± 3.56% (table S1).

The zeta potential values of bare Eth, Eth-HA, and Eth-HA-GC were + 20.9 ± 0.95, −16.2 ± 0.3, and + 38.0 ± 2.11 mV, respectively (Fig. 3d). These results indicated that HA and GC were successfully coated onto the surface of Eth via electrostatic adsorption. Also, the zeta potential and average diameter of Eth, Eth-HA and Eth-HA-GC were systematically investigated within one month. The results showed that just like the unmodified Eths, the one layer or bilayer coated Eths were all maintained monodispersity and did not rapidly change in size (Fig. S1), which should be mainly due to the mutual repulsion caused by the charges on their surface.

3.2. Cellular uptake of the eths by DCs in vitro

The uptake of Eths by DCs was observed with Confocal laser scanning microscopy assay. As shown in Fig. 4, the DiI-labeled Eth and Eth-HA-GC were engulfed by DCs and distributed in the cytoplasm around the nucleus. Obviously, DCs have preference for the uptake of Eth-HA-GC, and the amount of phagocytosis was much more than that of Eth-HA and non-modified Eth, suggesting that Eth-HA-GC has good ability to target DCs.

The BMDCs was co-cultured with the OVA-loaded Eths in vitro and

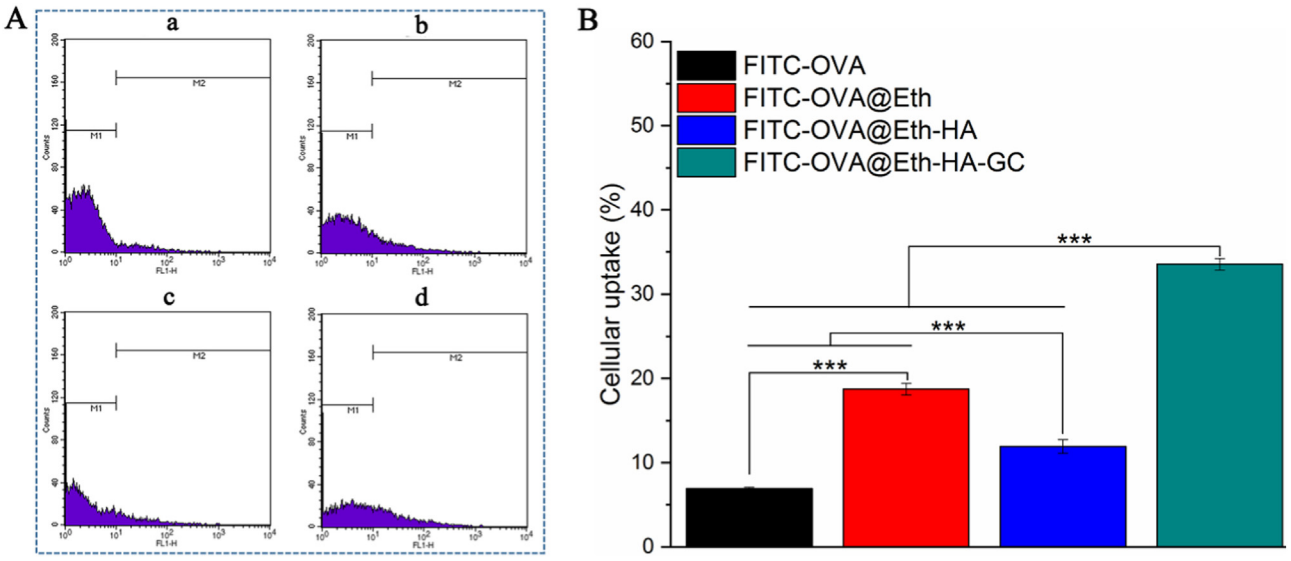

Fig. 5. Flow cytometry histograms (A) and percentage (B) of FITC-fluorescent signals in BMDCs after co-cultured with different carriers for 24 h (a: free FITC-OVA; b: FITC-OVA@Eth; c: FITC-OVA@Eth-HA; d: FITC-OVA@Eth-HA-GC).

analyzed using flow cytometry to further investigate the ability of the modified Eths to target DCs. As shown in Fig. 5 Aa & B, the cellular uptake of the free FITC-OVA was less, indicating that free OVA was difficult to enter into the cell through the cell membrane. The cellular uptake for the FITC-OVA encapsulated Eths were significantly increased compared with that of the free FITC-OVA (Fig. 5 A(b-d) & B). In particular, the cellular uptake for FITC-OVA@Eth-HA-GC was much better than that of other groups (Fig. 5 Ad & B).

3.3. In vitro inductive effect of DCs by the antigen-loaded eths

The ability of the modified Eths to induce DCs to mature and express immunoreactive cytokines was further investigated. The LPS-treated DCs was used as control. The flow cytometry results showed that PE fluorescence intensity for the group of OVA@Eth-HA-GC was significantly higher than that for the other groups (Fig. 6). Those results indicate that the antigen-loaded Eth-HA-GC has excellent ability to induce DCs to express CD11c, CD80 and CD86 which are the molecular marks related to maturation of DCs. The levels of TNF-α, IL-2 and IL-6 secreted by the BMDCs in the OVA@Eth, OVA@Eth-HA and OVA@Eth-HA-GC groups were significantly increased compared to that of the control and free OVA groups, and the OVA@Eth-HA-GC group has the highest level.

3.4. Characterization of the eths-loaded SF nanofibrous mats (ESNFM)

The concentration of aqueous SF solution in the electrospinning was set as 20% (*w/v*), and 2% (w/v) PEO was added to enhance the spinnability of the SF aqueous solution [17,31]. In this work, 25% of OVA (*w*/w based on SF) was added to the electrospinning solution. The

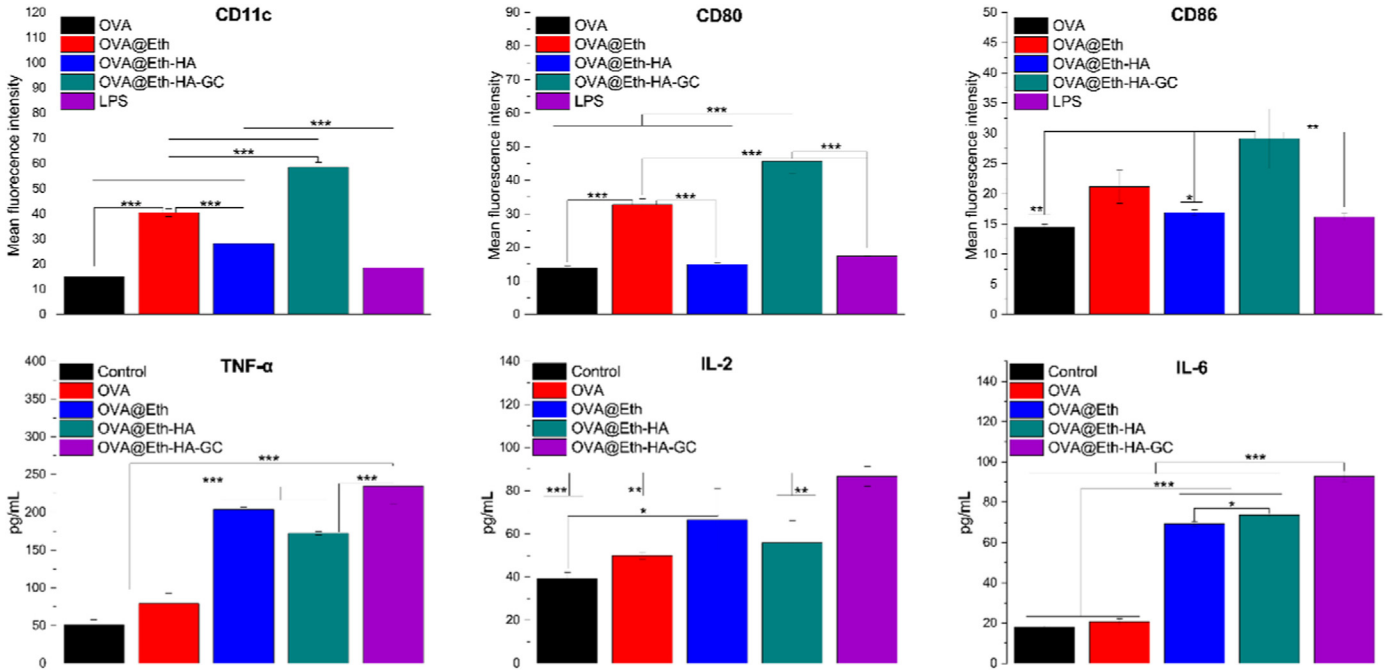

Fig. 6. The levels of CD11c, CD80, CD86, TNF-α, IL-2 and IL-6 secreted by BMDCs after co-culture with OVA-loaded Eths for 24 h.

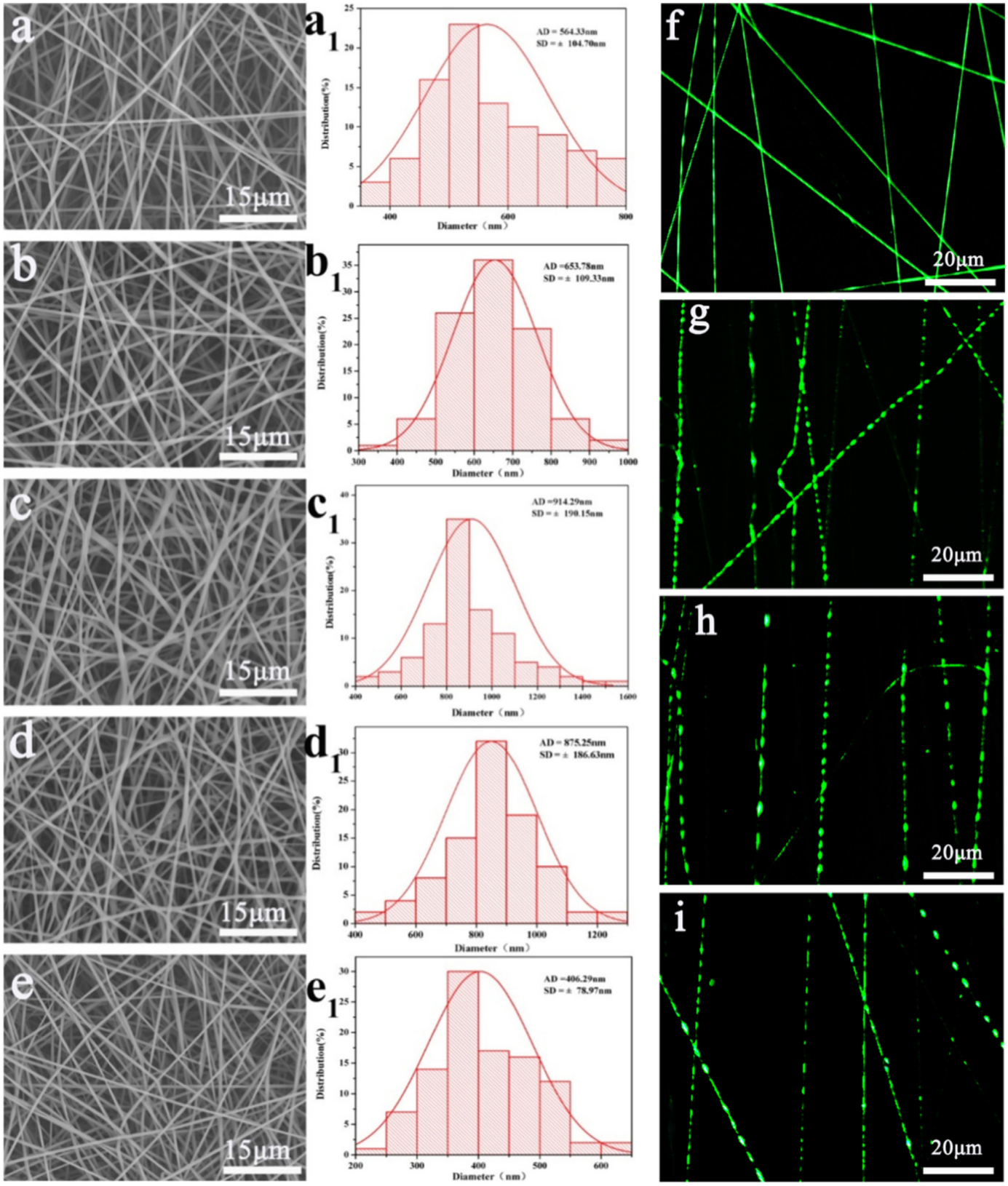

Fig. 7. SEM photograph (left column), diameter distribution (middle column) and fluorescence micrograph (right column) of the different SF patches (a: SF; b: OVA/SF; c: OVA@Eth/SF; d; OVA@Eth-HA/SF; e; OVA@Eth-HA-GC/SF; f: FITC-OVA/SF; g: FITC-OVA@Eth/SF; h: FITC-OVA@Eth-HA/SF; i: FITC-OVA@Eth-HA-GC/SF; a_1, b_1, c_1, d_1 and e_1 refer to the diameters of a, b, c, d and e respectively).

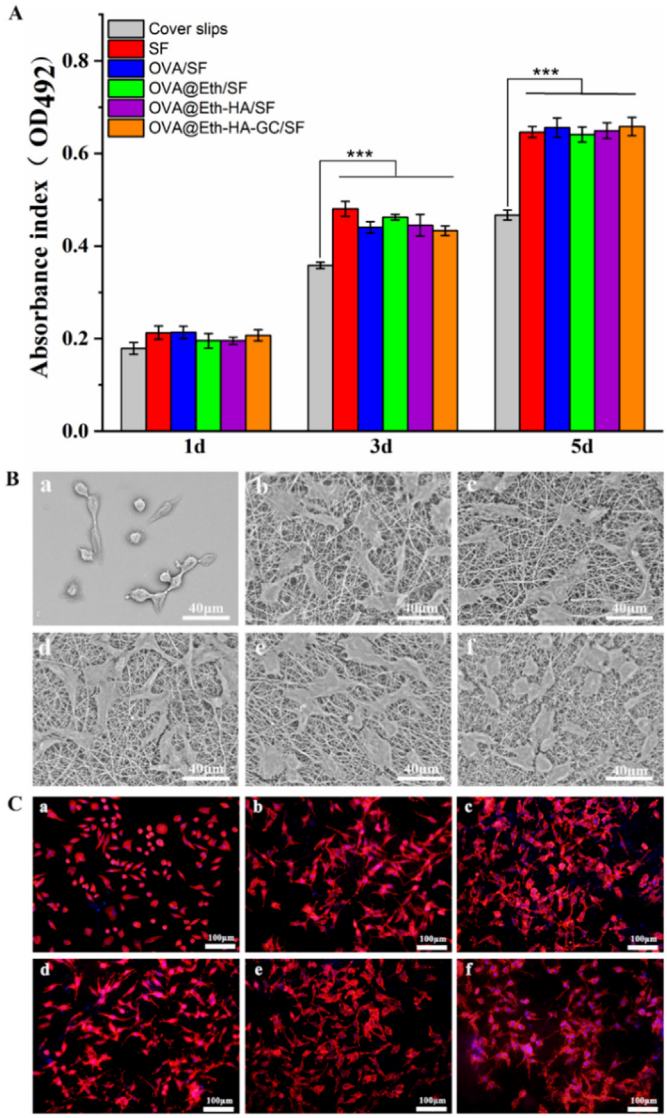

Fig. 8. Proliferation and morphology of L929 cells on different scaffolds(A: cell proliferation; B: SEM image of the cells; C: cells stained with rhodamine-labeled phalloidin and DAPI, phalloidin binds to F-actin to stain the microfilament red, and DAPI stains the nucleus blue; a: cover slip; b: SF; c: OVA@Eth/SF; d: OVA@Eth/SF; e: OVA@Eth-HA/SF; f: OVA@Eth-HA-GC/SF). (For interpretation of the references to color in this figure legend, the reader is referred to the web version of this article.)

nanofibers have a round and smooth morphology and the diameter of pure SF nanofibers is 564 ± 104 nm (Fig. 7). The incorporation of OVA does not change significantly the morphology of SF nanofibers but the diameter was increased to 653.78 ± 109.33 nm because the viscosity of the solution increased. The fiber diameters of OVA@Eth/SF increased to 914.29 ± 190.15 nm due to the Eths surface charge. However, the diameter of OVA@Eth-HA-GC/SF significantly reduced to 406.29 ± 78.97 nm, which may be due to the nature of the charge and surface tension of the GC.

The single-layer nanofibers loading FITC-OVA were observed using a fluorescence microscope to confirm the drug-loaded Eths was successfully loaded onto the nanofibers (Fig. 7f). The figure shows continuous uninterrupted linear green fluorescence appeared in the free FITC-OVA/SF nanofibers, while intermittent beaded green fluorescence appeared for the FITC-OVA@Eths-loaded fibers (Fig. 7g-i). Those results indicate that the FITC-OVA@Eths was successfully loaded onto the SF nanofibers and distributed evenly.

3.5. Cytocompatibility of the ESNFM

MTT assay was used to investigate the adhesion and proliferation of skin cells on the ESNFM (Fig. 8A). The L929 cells grown on the nanofibrous mats exhibit a higher viability than those on cover slips ($p < 0.05$), and there is no significant difference between neat SF and ESNFM. These results indicate that the ESNFM has good cytocompatibility and SF's biocompatibility was unaffected by the incorporation of Eths. The morphology of the cultured L929 cells was observed by SEM to confirm the cytocompatibility of the ELSNM. The result shows that cells cultured on both cover slips and the ELSNM have a good morphology and the cells on both the neat and ESNFM spread much better than those on cover slips (Fig. 8B). Moreover, cell-cell and cell-material interactions are seen clearly on the mats, which was presumed beneficial to signal transduction between cells and cells and between cells and materials (Fig. 8B b-f) [37,38]. A similar phenomenon was also observed under a fluorescence microscope (Fig. 8C). These results suggest that the as-prepared ESNFM has a good skin compatibility.

3.6. Transdermal performance of the ESNFM in vitro

The cumulative release of FITC-OVA in vitro for 48 h was examined to evaluate the transdermal performance of the ESNFM (Fig. 9A). The cumulative transdermal release of drugs from the ESNFM is greatly increased (up to 16%) compared to the group of FITC-OVA/SF. Moreover, the amount of drug retained in skin tissue from the ESNFM was significantly more than that from the FITC-OVA/SF group. The distribution of FITC-OVA in skin tissues was observed by fluorescence microscopy (Fig. 9B&C). The results show that the green fluorescence intensity of FITC-OVA/SF group was much lower than that of the ESNFMs, which is consistent with the cumulative release data. The dynamic transdermal progress of the Eths was investigated by continuously observing the distribution of Eths in the skin at different time points. As shown in Fig. S4, the DiI-labeled Eths gradually penetrated from the surface to the deep layers of skin. These data confirmed the remarkable ability of Eths to penetrate the stratum corneum.

3.7. Evaluation of the TCI effect induced by the OVA-loaded ESNFM

To investigate whether the antigen-loaded ESNFM has the ability to induce a systemic antigen-specific antibody response, mice were immunized twice with the OVA-loaded mats through transdermal route (Fig. 10). Serum samples were collected and anti-OVA antibodies were measured on day 14 after immunization. Mice that treated with OVA/SF had a low level of OVA-specific IgG antibody, like the untreated control. However, much higher levels of OVA-specific IgG were observed in the serum from the mice treated with the OVA-loaded ESNFMs via the transdermal route ((Fig. 10). Furthermore, the level of OVA-specific IgG from the OVA@Eth-HA-GC/SF treated mice was significantly higher than that from the mice treated with OVA@Eth/SF. These results prove that the effective targeted delivery of antigen to DCs in the skin leading to more effective humoral immune response.

To assess whether OVA@Eth-HA-GC trigger the immune response toward a Th1 or Th2 immune response, spleen cells from mice were obtained 1 week after the final immunization and cultured with 10 μg/mL OVA for 72 h. The quantity of cytokines (IFN-γ for Th1, IL-2 and IL-6 for Th2) in the culture supernatants was determined by ELISA (Fig. 10b-d). The IFN-γ production was significantly increased in spleen cells from mice treated with the OVA@Eth/SF compared to that induced by OVA/SF (Fig. 10 b). Furthermore, the spleen cells from mice treated with OVA@Eth-HA-GC/SF show a significant increase in the production of IL-2 and IL-6 compared to other groups (Fig. 10B b&c). In conclusion, the transdermal administration of OVA@Eth-HA-GC/SF induced higher secretions of both Th1 and Th2 cytokines and an effective immune response to OVA.

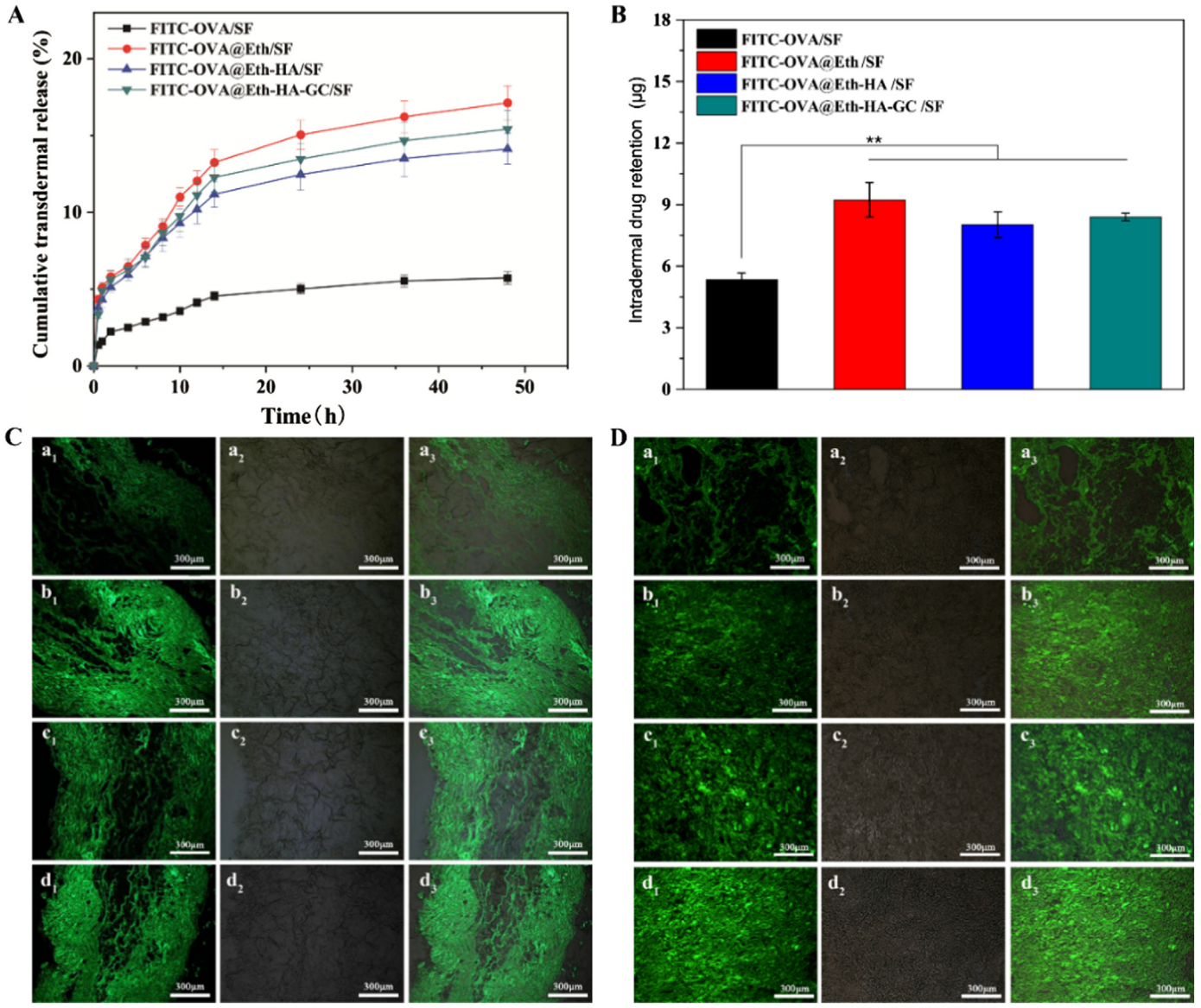

Fig. 9. Transdermal performance of the mats in vitro (A: cumulative transdermal release curve; B: intradermal drug retention; C: cross section of the skin after treatment with different mats; D: longitudinal section of the skin after treatment with different mats; a: FITC-OVA/SF; b: FITC-OVA@Eth/SF; c: FITC-OVA@Eth-HA/SF; d: FITC-OVA@Eth-HA-GC/SF; 1: fluorescent photo; 2: photomicrograph; 3: merge of fluorescent photo and photomicrograph).

3.8. The protective effect of immune response induced by the OVA-loaded ESNFM against EG7 tumor challenge in mice model

The mice were immunized with the OVA-loaded ESNFMs three times at 1-week intervals to evaluate whether the ESNFM could be used as a DC-targeted transdermal vaccine to induce protective immune response against EG7 tumor challenge (Fig. 11). Mice were subcutaneously injected with E.G7-OVA cells 14 days after the second immunization and tumor growth was evaluated in each mouse for 5 weeks. The solid tumors began to appear on the 8th day after tumor inoculation, and the volume of the tumor increased with time (Fig. 11A). On the 16th day, the tumor volume of each group began to differ. The volumes of the tumor from the control and OVA/SF groups were similar and increased rapidly. While the tumor volumes from the mice treated with OVA@Eth-HA-GC/SF increased significantly slower and the 28-day difference is more pronounced. Fig. 11B shows the tumor entities on the 28th day after tumor inoculation in each group. Obviously, the tumor volume of the OVA@Eth-HA-GC/SF group is much smaller than that of other groups. These results indicate that the DCs-targeting and immunostimulatory effects of the OVA@Eth-HA-GC/SF can successfully induce a systemic immune response that protects mice against tumor challenge.

4. Discussion

TCI is a new strategy for needle-free vaccination that delivers specific antigens to the APCs - mainly DCs present in the active epidermis and dermis in the skin - to elicit an effective immune response [1–3]. Compared with subcutaneous or intramuscular injection, the TCI vaccine patch has various advantages such as good compliance, high efficiency, easy operation, easy storage and transportation, and avoiding the liver first-pass effect [1,2]. The main goal of TCI is formulating an antigen-loaded carrier capable of penetrating the SC and targeting DCs as the SC is a difficult barrier for free macromolecular antigens. Eth is an ideal transdermal drug delivery vehicle for its advantages such as smaller particle size, high encapsulation rate, higher skin permeability and better fluidity and stability [5–12]. The electrospun nanofibrous mats have been regarded as useful drug delivery systems for their

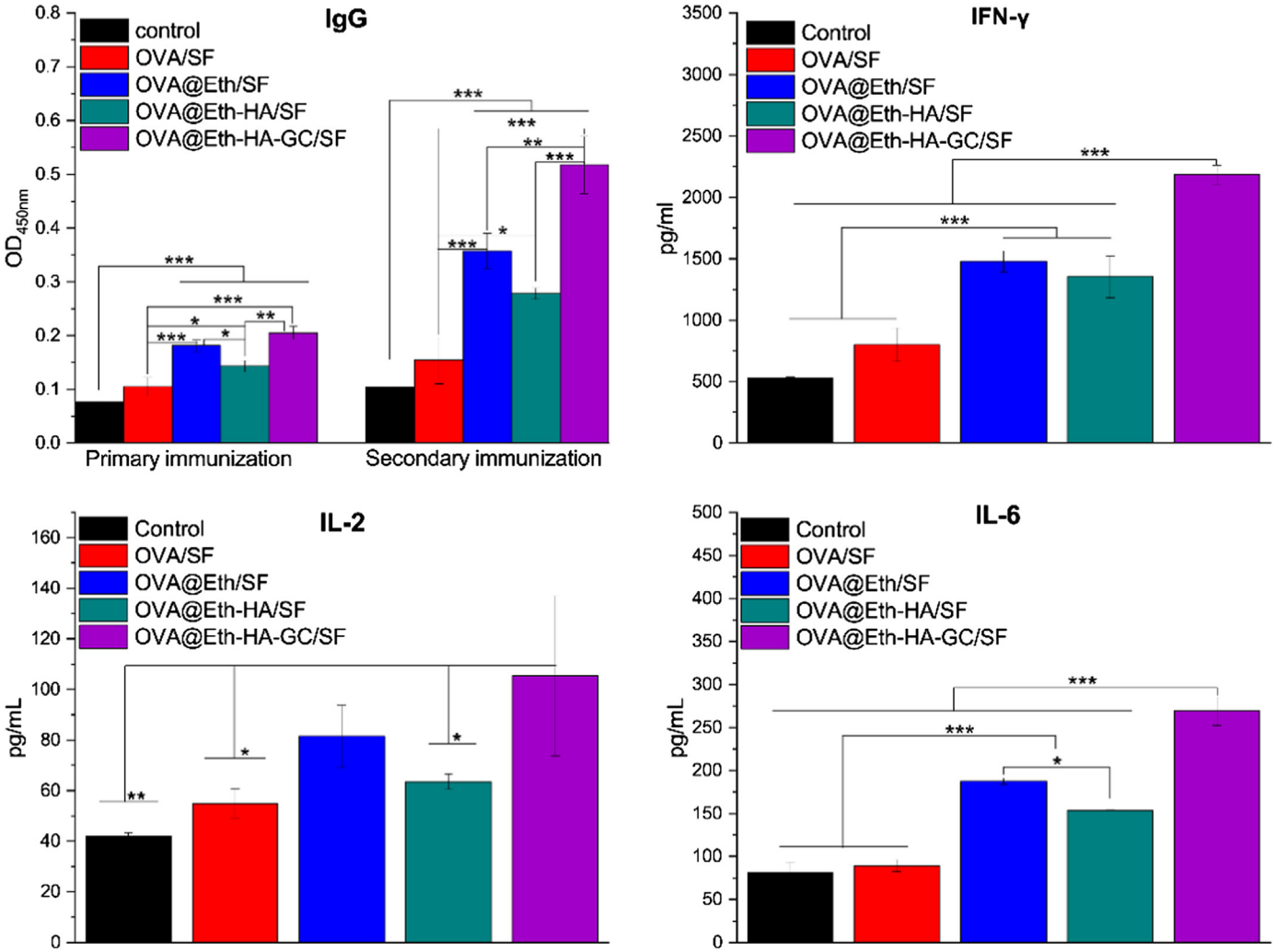

Fig. 10. The levels of serum OVA-specific IgG and spleen cell-derived cytokines (IFN-γ, IL-2 and IL-6) from the mice received transcutaneous immunization.

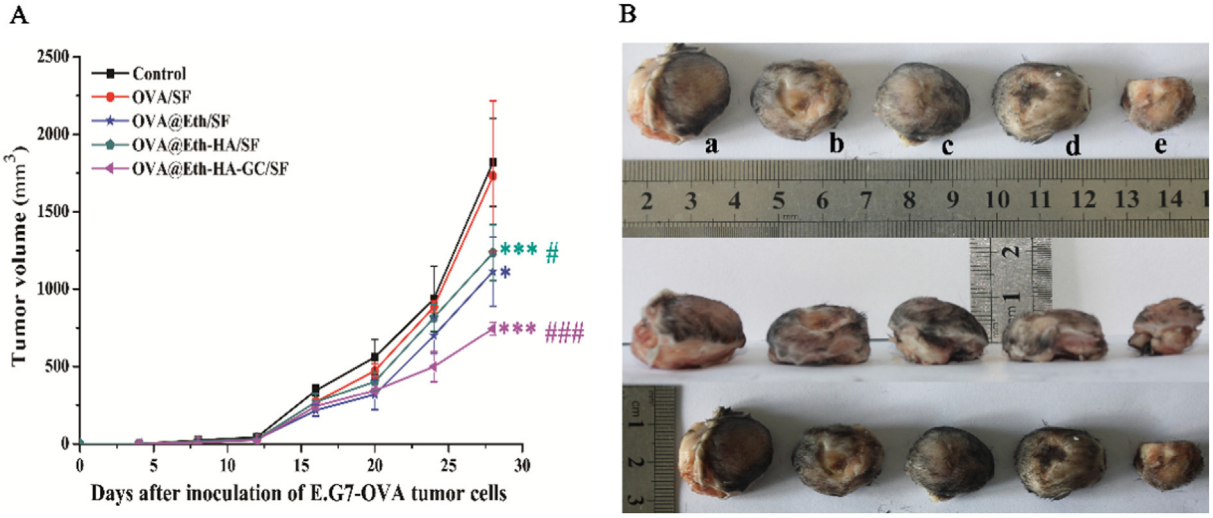

Fig. 11. The tumor growth curve (A) and tumor photos at day 28 (B) after transcutaneous immunization by OVA-loaded mats (a: control group; b: OVA/SF group; c: OVA@Eth/SF group; d: OVA@Eth-HA/SF group; e: OVA@Eth-HA-GC/SF group; * Significant difference compared with the control group; # significant difference compared with the OVA/SF group).

desirable features – such as high surface area-to-volume ratios and porosity with interconnectivity - that play a critical role in mass transport and provide efficient drug delivery [14]. Our previous studies have confirmed the good performance of the electrospun SF nanofibrous mats in drug delivery [17,31,39–42]. We demonstrated that Eth-loaded SF nanofibrous mats (ESNFM) can efficiently deliver biomacromolecules (molecular weight greater than 60,000) into mice through the transdermal route (Fig. S2). In addition to the properties of Eth, the large specific surface area of nanofibers should also contribute to the good transdermal performance of the ESNFM by enlarging the contact area between the Eths and the SC of the skin. Therefore, the ESNFM can be a good solution for transdermal drug delivery and TCI.

Galactosyl has been reported to specifically recognize and interact with the GCL receptors on the DCs surface, thus the galactosylated nanocarriers can target DCs and stimulate their maturation [19–22]. GC has a good performance on promoting hepatocytes adhesion and proliferation as it contains galactosyl and is positively charged [23–25]. In this study, HA and GC were used to modify the Eth via electrostatic adsorption to bring the galactosyl group on the surface for targeting DCs. The results show that Eth-HA-GC is positively charged, which is beneficial to adsorption of negatively charged drugs (such as protein and DNA) and delivering them into cells through fusing with the negatively charged cell membrane. In vitro data showed that the uptake of Eth-HA-GC by BMDCs is much more than that of Eth-HA or bare Eth (Fig. 4**&5**), which confirmed that the presence of GC has given Eths the ability to target DCs. Moreover, the expression of CD11c, CD80 and CD86 stimulated by the OVA@Eth-HA-GC is also more (Fig. 6). CD11c is one of the markers expressed by DCs at its earlier stage, while CD80 and CD86 belong to the ones expressed by the mature DCs [20,43]. Therefore, our results demonstrate that Eth-HA-GC is a good nanocarrier for antigens to target DCs and stimulate them to mature. Also, the antigen-loaded Eth-HA-GC significantly enhanced DCs' secretion of TNF-α, IL-2 and IL-6. Since these cytokines are pro-inflammatory factors which can further induce the activation and proliferation of T cells [44,45], our results suggest that the antigen-loaded Eth-HA-GC can effectively stimulate a cellular immune response.

Encouraged by the impressive data shown in Fig. 4-6, we fabricated a novel antigen-loaded ESNFM named OVA@Eth-HA-GC/SF by a green electrospinning process. This unique ESNFM had excellent skin cytocompatibility and showed a good transdermal performance. The transdermal efficiency of Eths has a slight decrease after modification with HA and GC, which might be mainly due to the increase of the particle size. HA-modified Eth has recently been reported to have a better transdermal performance than bare Eth due to HA's unique function that increasing the moisture content of the cuticle to make it expand and then reduce the compactness of its structure [26]. Here, the situation is some different – the Eth-HA showed an inferior transdermal performance to the bare Eth and Eth-HA-GC, which should be attributed to surface charged property besides particle size. The prepared Eth and Eth-HA-GC in this study are positively charged, while Eth-HA negatively charged. The positively charged surface facilitates the carriers' adhesion to the negatively charged cell membrane, which is beneficial to the skin permeation performance.

The fluorescence intensity of BMDCs co-cultured with FITC-OVA@Eth-HA-GC/SF is much higher than that with FITC-OVA@Eth-HA and FITC-OVA@Eth (**Fig. S3**), which is consistent with the results of BMDCs co-cultured with free Eths and also indicate that the Eths can be released from the ESNFMs. Furthermore, in vivo results showed that the treatment of OVA@Eth-HA-GC/SF significantly increase levels of OVA-specific antibody in serum and that of IFN-γ, IL-2 and IL-6 secreted by spleen cells, which indicates that OVA@Eth-HA-GC/SF can effectively stimulate both humoral and cellular immune responses. Since IFN-γ and IL-2 belong to Th1 type cytokines, and IL-6 is one of the Th2 cytokines, these data demonstrate the OVA@Eth-HA-GC/SF can induce effective Th1 and Th2 cellular and humoral immune response [20,46,47]. The tumor inhibitory test was conducted with a mouse model to further investigate the TCI effect of OVA@Eth-HA-GC/SF. The results indicated that the transdermal administration of OVA@Eth-HA-GC/SF significantly inhibits the growth of E.G7 tumor. Our data demonstrates that the OVA@Eth-HA-GC/SF nanofibrous mats can stimulate an effective immune response through transdermal route.

Considering all the results in this study, as well as the simple process and environmental friendliness of its preparation, the TCI system based on the Eth-HA-GC/SF nanofibrous mats has a promising application potential in immunization and tumor treatment.

5. Conclusion

In this study, we report a galactosylated ethosome (Eth-HA-GC) that has the ability to target DCs and stimulate them to mature. A novel SF nanofibrous mats loading Eth-HA-GC (Eth-HA-GC/SF) fabricated via green electrospinning shows a good performance in transdermal delivery of macromolecular antigens. The transdermal administration of OVA-loaded Eth-HA-GC/SF (OVA@Eth-HA-GC/SF) significantly increase the levels of serum IgG antibody and Th1/Th2 cytokines in mice. Also, the mice treated with OVA@Eth-HA-GC/SF through transdermal route show an efficient anti-OVA immune response against EG7 tumor challenge. Our results suggest the transdermal vaccination with the antigen-loaded Eth-HA-GC/SF nanofibrous mats could effectively elicit cellular and humoral immune responses and systemic anti-tumor immunity. Therefore, this novel Eth-HA-GC/SF nanofibrous mats could find a promising application in the fields of TCI and antitumor.

Acknowledgements

This research was supported by Shanghai Science and Technology Committee Project (18490740400), National Natural Science Fund of China (81671586 and 31900949), The National Key Research and Development Program of China (2018YFC1706200) and the Fundamental Research Funds for the Central Universities (2232019D3-20).

Appendix A. Supplementary data

Supplementary data to this article can be found online at https://doi.org/10.1016/j.jconrel.2020.07.047.

References

[1] Laura Engelke, Gerhard Winter, Sarah Hook, Julia Engert, Recent insights into cutaneous immunization: how to vaccinate viathe skin, Vaccine 33 (2015) 4663–4674.
[2] Kevin Ita, Transdermal delivery of vaccines-recent progress and critical issues, Biomed. Pharmacother. 83 (2016) 1080–1088.
[3] Eduardo J. Villablanca, Jorge R. Mora, A two-step model for Langerhans cell migration to skin-draining LN, Eur. J. Immunol. 38 (2008) 2975–2980.
[4] N. Li, L.H. Peng, X. Chen, S. Nakagawa, J.Q. Gao, Transcutaneous vaccines: novel advances in technology and delivery for overcoming the barriers, Vaccine 29 (2011) 6179–6190.
[5] Z. Chen, Y. Lv, J. Qi, Q. Zhu, Y. Lu, W. Wu, Overcoming or circumventing the stratum corneum barrier for efficient transcutaneous immunization, Drug Discov. Today 23 (2018) 181–186.
[6] L.N. Shen, Y.T. Zhang, Q. Wang, et al., Enhanced in vitro and in vivo skin deposition of apigenin delivered using ethosomes, Int. J. Pharm. 460 (2014) 280–288.
[7] Y. Rao, F. Zheng, X. Zhang, J. Gao, W. Liang, In vitro percutaneous permeation and skin accumulation of finasteride using vesicular ethosomal carriers, AAPS PharmSciTech 9 (2008) 860–865.
[8] Y. Wo, Z. Zhang, Y. Zhang, et al., Preparation of ethosomes and deformable liposomes encapsulated with 5-fluorouracil and their investigation of permeability and retention in hypertrophic scar, J. Nanosci. Nanotechnol. 11 (2011) 7840–7847.
[9] L. Yang, L. Wu, D. Wu, D. Shi, T. Wang, X. Zhu, Mechanism of transdermal permeation promotion of lipophilic drugs by ethosomes, Int. J. Nanomedicine 12 (2017) 3357–3364.
[10] M.M. Elsayed, O.Y. Abdallah, V.F. Naggar, et al., Deformable liposomes and ethosomes: mechanism of enhanced skin delivery, Int. J. Pharm. 322 (2006) 60–66.
[11] E. Touitou, N. Dayan, L. Bergelson, et al., Ethosomes - novel vesicular carriers for enhanced delivery: characterization and skin penetration properties, J. Control. Release 65 (2000) 403–418.

[12] Varun Garg, Harmanpreet Singh, Sneha Bimbrawh, Sachin Kumar Singh, Monica Gulati, Yogyata Vaidya, Prabhjot Kaur, Ethosomes and Transfersomes: principles, perspectives and practices, Curr. Drug Deliv. 14 (2017) 613–633.
[13] M.M. Stevens, J.H. George, Exploring and engineering the cell surface interface, Science 310 (2005) 1135–1138.
[14] R. Goyal, L.K. Macri, H.M. Kaplan, J. Kohn, Nanoparticles and nanofibers for topical drug delivery, J. Control. Release 240 (2016) 77–92.
[15] M. Kulkarni, U. Greiser, T. O'brien, et al., Liposomal gene delivery mediated by tissue-engineered scaffolds, Trends Biotechnol. 28 (2010) 28–36.
[16] L. Fan, J.L. Li, Z. Cai, X. Wang, Creating biomimetic anisotropic architectures with co-aligned nanofibers and macrochannels by manipulating ice crystallization, ACS Nano 12 (2018) 5780.
[17] Dongdong Zhang, Linpeng Fan, Linlin Ma, Junqiu Liu, Kai Zhou, Xinran Song, Meiqi Sun, Xiumei Mo, Chuanglong He, Yuxin Chen, Hongsheng Wang, Helicobacter pylori ribosomal protein-A2 peptide/silk fibroin Nanofibrous composites as potential wound dressing, J. Biomed. Nanotechnol. 15 (2019) 507–517.
[18] N. Romani, M. Thurnher, J. Idoyaga, et al., Targeting of antigens to skin dendritic cells: possibilities to enhance vaccine efficacy, Immunol. Cell Biol. 88 (2010) 424–430.
[19] H.W. Wang, P.L. Jiang, S.F. Lin, et al., Application of galactose-modified liposomes as a potent antigen presenting cell targeted carrier for intranasal immunization, Acta Biomater. 9 (2013) 5681–5688.
[20] P.L. Jiang, H.J. Lin, H.W. Wang, et al., Galactosylated liposome as a dendritic cell-targeted mucosal vaccine for inducing protective anti-tumor immunity, Acta Biomater. 11 (2015) 356–367.
[21] S. Ebner, Z. Ehammer, S. Holzmann, P. Schwingshackl, M. Forstner, P. Stoitzner, G.M. Huemer, P. Fritsch, N. Romani, Expression of C-type lectin receptors by subsets of dendritic cells in human skin, Int. Immunol. 16 (2004) 877–887.
[22] N. Higashi, K. Fujioka, K. Denda-Nagai, S. Hashimoto, S. Nagai, T. Sato, Y. Fujita, A. Morikawa, M. Tsuiji, M. Miyata-Takeuchi, Y. Sano, N. Suzuki, K. Yamamoto, K. Matsushima, T. Irimura, The macrophage C-type lectin specific for galactose/N-acetylgalactosamine is an endocytic receptor expressed on monocyte-derived immature dendritic cells, J. Biol. Chem. 277 (2002) 20686–20693.
[23] I.K. Park, J. Yang, H.J. Jeong, H.S. Bom, I. Harada, T. Akaike, S.I. Kim, C.S. Cho, Galactosylated chitosan as a synthetic extracellular matrix for hepatocytes attachment, Biomaterials 24 (2003) 2331–2337.
[24] Z.Q. Feng, X. Chu, N.P. Huang, et al., The effect of nanofibrous galactosylated chitosan scaffolds on the formation of rat primary hepatocyte aggregates and the maintenance of liver function, Biomaterials 30 (2009) 2753–2763.
[25] T.W. Chung, J. Yang, T. Akaike, K.Y. Cho, J.W. Nah, S.I. Kim, C.S. Cho, Preparation of alginate/galactosylated chitosan scaffold for hepatocyte attachment, Biomaterials 23 (2002) 2827–2834.
[26] Jiesi Xie, Yujie Ji, Wei Xue, Dong Ma, Yunfeng Hu, Hyaluronic acid-containing ethosomes as a potential carrier for transdermal drug delivery, Colloids Surf. B Biointerfaces 172 (2018) 323–329.
[27] Y. Gao, X. Cheng, Z. Wang, J. Wang, T. Gao, P. Li, et al., Transdermal delivery of 10,11-methylenedioxycamptothecin by hyaluronic acid based nanoemulsion for inhibition of keloid fibroblast, Carbohydr. Polym. 112 (2014) 376–386.
[28] H.S. Jung, K.S. Kim, S.H. Yun, S.K. Hahn, Enhancing the transdermal penetration of nanoconstructs: could hyaluronic acid be the key? Nanomedicine 9 (2014) 743–745.
[29] L. Ma, X. Wang, J. Wu, D. Zhang, L. Zhang, X. Song, H. Hong, C. He, X. Mo, S. Wu, G. Kai, H. Wang, Polyethylenimine and sodium cholate-modified ethosomes complex as multidrug carrier for the treatment of melanoma through transdermal delivery, Nanomedicine (Lond). 14 (2019) 2395–2408.
[30] M.B. Lutz, N. Kukutsch, A.L. Ogilvie, S. Rossner, F. Koch, N. Romani, G. Schuler, An advanced culture method for generating large quantities of highly pure dendritic cells from mouse bone marrow, J. Immunol. Methods 223 (1999) 77–92.
[31] Xingxing Yang, Linpeng Fan, M.A. Linlin, Yunyi Wang, Si Lin, Fan Yu, Xiaohan Pan, Gejie Luo, Dongdong Zhang, Wang Hong-Sheng, Green electrospun Manuka honey/silk fibroin fibrous matrices as potential wound dressing, Mater. Des. 119 (2017) 76–84.
[32] K. Jagadeeswara Reddy, K.T. Karunakaran, Purification and characterization of hyaluronic acid produced by Streptococcuszooepidemicus strain 3523-7, J. BioSci. Biotech. 2 (2013) 173–179.
[33] Siddhodhan S. Bodade, Karimunnisa Sameer Shaikh, Meghana S. Kamble, Praveen D. Chaudhari, A study on ethosomes as mode for transdermaldelivery of an anti-diabetic drug, Drug Deliv. 20 (2013) 40–46.
[34] Can Zhang, Qineng Ping, Ding Ya, Yao Cheng, Jian Shen, Synthesis, characterization, and microsphere formation ofGalactosylated chitosan, J. Appl. Polym. Sci. 91 (2004) 659–665.
[35] S. Jeon, C.Y. Yoo, S.N. Park, Improved stability and skin permeability of sodium hyaluronate-chitosan multilayered liposomes by layer-by-layer electrostatic deposition for quercetin delivery, Colloids Surf B Biointerfaces 129 (2015) 7–14.
[36] Z.S. Haidar, R.C. Hamdy, M. Tabrizian, Protein release kinetics for core-shell hybrid nanoparticles based on the layer-by-layer assembly of alginate and chitosan on liposomes, Biomaterials 29 (2008) 1207–1215.
[37] D.H. Roh, J. Mater. Sci. Mater. Med. 17 (2006) 547–552.
[38] C. Sobajo, F. Behzad, X.F. Yuan, A. Bayat, Silk: a potential medium for tissue engineering, Eplasty 8 (2008) 438–446.
[39] Linlin Ma, Dongdong Zhang, Xingxing Yang, Lin Zhang, Jin Chu, Guoyin Kai, Chuanglong He, Xiumei Mo, Hongsheng Wang, Cirsium Japonicum DC ingredients-loaded silk fibroin nanofibrous matrices with excellent hemostatic activity, Biomed. Phys. Eng. Express 4 (2018) 025035.
[40] Si Lin, Mengxia Chen, Huayue Jiang, Linpeng Fan, Binbin Sun, Fan Yu, Xingxing Yang, Xiangxin Lou, Chuanglong He, Hongsheng Wang, Green electrospun grape seed extract-loaded silk fibroin nanofibrousmats with excellent cytocompatibility and antioxidant effect, Colloids Surf. B: Biointerfaces 139 (2016) 156–163.
[41] L. Fan, Z. Cai, K. Zhang, F. Han, J. Li, C. He, X. Mo, X. Wang, H. Wang, Green electrospun pantothenic acid/silk fibroin composite nanofibers: fabrication, characterization and biological activity, Colloids Surf. B: Biointerfaces 117 (2014) 14–20.
[42] X. Sheng, L. Fan, C. He, K. Zhang, X. Mo, H. Wang, Vitamin E-loaded silk fibroin nanofibrous mats fabricated by green process for skin care application, Int. J. Biol. Macromol. 56 (2013) 49–56.
[43] J. Banchereau, F. Briere, C. Caux, J. Davoust, S. Lebecque, Y.J. Liu, et al., Immunobiology of dendritic cells, Annu. Rev. Immunol. 18 (2000) 767–811.
[44] Y.J. Liu, H. Kanzler, V. Soumelis, M. Gilliet, Dendritic cell lineage, plasticity and cross-regulation, Nat. Immunol. 2 (2001) 585–589.
[45] O. Dienz, M. Rincon, The effects of IL-6 on CD4 T cell responses, Clin. Immunol. 130 (2009) 27–33.
[46] S. Romagnani, T-cell subsets (Th1 versus Th2), Ann. Allergy Asthma Immunol. 85 (2000) 9–18.
[47] Christopher S. Garris, Sean P. Arlauckas, Rainer H. Kohler, Alfred Zippelius, Ralph Weissleder, Mikael J. Pittet, Successful anti-PD-1 Cancer immunotherapy requires T cell-dendritic cell crosstalk involving the cytokines IFN-g and IL-12, Immunity 49 (2018) 1–14.